

Radiation dose distribution inside interaction chamber in PW laser facilities during laser-plasma proton acceleration experiments and method to increase the proton energy spectrum measurement resolution

A. Groza¹, E. Stancu^{3,6}, A. Chiroasca^{1,5}, B. Butoi¹, D.B. Dreghici^{1,5}, M. Serbanescu^{2,7},
O. Stoican⁴, C. Ticos⁸, B. Mihalcea¹ and M. Ganciu^{1*}

¹ National Institute for Laser, Plasma and Radiation Physics (INFLPR), Low Temp. Plasma Dept., Atomistilor Str. No. 409, 077125 Magurele, Ilfov County, Romania

² National Institute for Laser, Plasma and Radiation Physics, Centre for Advanced Laser Technology (CETAL-PW), Atomistilor Str. No. 409, 077125 Magurele, Ilfov County, Romania

³ National Institute for Laser, Plasma and Radiation Physics, STARDOOR Dept., Atomistilor Str. No. 409, 077125 Magurele, Romania

⁴ National Institute for Laser, Plasma and Radiation Physics (INFLPR), Plasma Physics and Nuclear Fusion Laboratory, Atomistilor Str. No. 409, 077125 Magurele, Ilfov County, Romania

⁵ Faculty of Physics, University of Bucharest, Nuclear Phys. Dept. Magurele, Romania

⁶ Faculty of Physics, University of Bucharest, Doctoral School in Physics, Magurele, Romania

⁷ Politehnica University of Bucharest (UPB), Faculty of Electronics, Telecommunications and Information Technology Splaiul Independentei 313, Bucharest 060042, Romania

⁸ National Institute for Laser, Plasma and Radiation Physics, (INFLPR), Accelerator Dept., Atomistilor Str. No. 409, 077125 Magurele, Romania

* Correspondence: mihai.ganciu@inflpr.ro;

Abstract

The map of the radiation dose distribution has been determined experimentally inside the interaction chamber during high-power laser - thin solid target experiments. In addition, the map also has been assessed theoretically by performing 3D simulations. Maximum values of the integrated doses of tens of mGy/shot are recorded in a direction normal to the target, at a distance of about 30 cm apart from the laser-target interaction point. Monte-Carlo simulation of the radiation doses map around the laser-foil interaction point is performed using Geant4 General Particle Source code and the particular geometry chosen for the experimental setup. The computed radiation dose distribution shows a good agreement with experimental results, and this represents the most important progress made within the contract. We introduce a new method to increase the measurement resolution of the proton energy spectrum, based on using a stack of thin solid detectors, preferably CR-39 [OSIM Patent Application, A/00337/05-06-19]. Each detector is thinner than the Bragg peak region that characterizes the loss of kinetic energy as a function of the particle penetration depth in the detector materia. The thick ness of the Bragg peak region is defined as the full width at half maximum (FWHM) of the energy loss curve, that describes the specific energy deposition dE/dx of a heavy charged particle as a function of the penetration depth x .

2. Introduction

Space weather represents a branch of space physics and aeronomy (heliophysics), that deals with the investigation of the continuously changing environment conditions characteristic to the Solar system. It includes study of phenomena that occur in the magnetosphere, ionosphere, thermosphere and exosphere.

Space weather is determined by the solar wind and the interplanetary magnetic field (IMF) carried by the solar wind hot plasma [1]. A variety of physical phenomena are associated with space weather, including geomagnetic storms, or constant remodelling of the Van Allen radiation belts caused by interplanetary shock waves - an outburst of highly energetic particles carried by the solar wind which can literally blast away the outer radiation belt and then split its remains into two distinct rings [2]. Other phenomena associated with space weather are ionospheric disturbances and scintillation of satellite-to-ground radio signals and long-range radar signals [3], auroras and geomagnetically induced currents at Earth's surface. Coronal mass ejections (CMEs) and the associated shock waves can also result in major perturbation of space weather, as they can compress the magnetosphere and trigger geomagnetic storms. Solar energetic particles (SEP) accelerated by coronal mass ejections or solar flares can trigger solar particle events (SPEs), a critical parameter with respect to the impact of space weather on humans, as they can inflict damage on electronics onboard spacecraft, endanger the lives of astronauts, or increase radiation hazards for high-altitude, high-latitude air flights.

Spacecraft charging, the accumulation of electrostatic charge on non-conducting materials at the spacecraft surface due to low energy particles, is one of the predominant space weather effects on an orbiting spacecraft [4]. Another harmful effect is the exposure of the human body to space radiation (ionizing radiation) [1, 4]. Preliminary results obtained in INFLPR show that simple electronic circuits introduced in a 6 MeV electron beam are rendered inoperable by a dose of $100 \div 300$ Gy delivered within a few seconds [5].

Conditions similar to those found around space stations and spacecraft can be achieved using high power/high intensity lasers [6, 7]. High intensity lasers have been used more and more in nowadays research, for the study of matter under extreme conditions and for laser driven particle acceleration. The high intensity laser pulse generates a plasma at the target surface, and then interacts with it. The plasma can accelerate electrons up to energies of tens of MeV [6, 7, 8]. The “hot” electrons and laser accelerated electrons interact with the target chamber walls, generating X-ray bremsstrahlung photons. The mixed field of photons and electrons might create a radiation hazard associated with such laser-matter interaction experiments [6].

Thus, different ionizing particle types and doses can be obtained in high power laser - thin solid target experiments. For example, protons with energies up to tens of MeV and mixed fields of electrons and photons with doses of tens of mGy/shot can be generated, depending on the target thickness and material [6, 7]. Appropriate experimental conditions can be achieved at several high power laser facilities worldwide [9, 10, 11].

In the current progress report we present measurements of integrated doses produced by the mixed field of electrons and X-ray photons generated during high power laser-thin solid target interaction experiments, in which laser accelerated protons with energies up to about 14 MeV [12, 13] were demonstrated by using the CETAL high power laser facility [10].

3.1. Experimental setup

Mapping of the radiation dose inside the target chamber has been performed during experiments of high power laser - thin solid target interaction, for a laser intensity in focus of about 5×10^{19} W/cm² (40 fs pulse duration [14]). The laser incidence angle with respect to the target normal is 45°. The laser spot area is about (9×23) 207 μm^2 , and the fraction of energy within FWHM of the laser spot is approximately 30 %. Experimental dose assessment is carried out using passive detectors, such as CR-39 and EBT-3 radiochromic films (RCF) [13], while theoretical estimations of the dose map inside the interaction chamber are performed using the radiation transport software Geant 4 V.10.5 [15]. The experimental set-up shown in Figure 1 has been designed with an aim to allow a straightforward analysis of laser accelerated electron and proton beams. It consists of the target and passive detectors holder assembly, a magnetic spectrometer, and an optical analysis system. The magnetic spectrometer is used to estimate the electron beam energy. The target and detector holder system consists of two parallel metal plates centred using a horizontal metal axle. The targets are positioned on the first plate, while the passive detectors used for proton beam analysis are essentially placed on the second plate, where they alternate with holes.

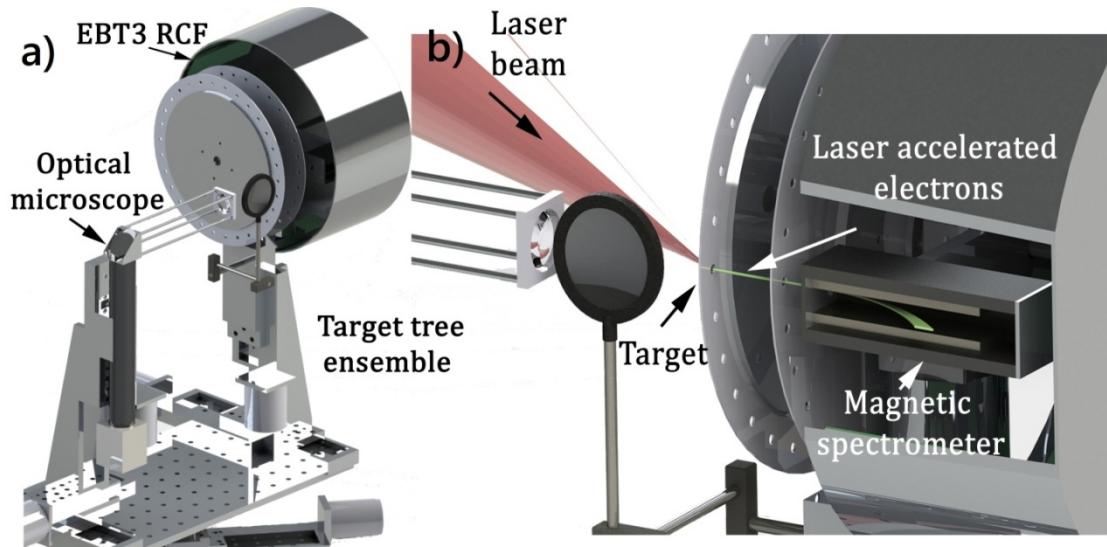


Figure 1: a) Experimental setup; b) Detailed view of the experimental setup.

Near the magnetic spectrometer a rotatable metal cylinder is placed, that acts as a holder for the EBT3 radiochromic films used to estimate the energy of laser accelerated electrons (~ 14 MeV). The target and detector holder assembly are placed on mechanical translation and rotation stages, to achieve precise alignment in the laser beam focus. The optical analysis system is described in detail in Ref. [13]. To measure the dose distribution inside the target chamber, 2×2 cm² passive EBT3 radiochromic film detectors (covered with a 10 μ m thick aluminum foil) are placed at different positions near the experimental setup, as illustrated in Fig. 1.

3.2 Method for dose estimation using radiochromic films (RCF)

The dosimetry assessment performed during high power laser - thin solid target interaction experiments by means of EBT3 radiochromic films supplies information about the two dimensional (2D) radiation dose distribution. The EBT3 films present a symmetrical layer structure, as the active layer (28 μ m thick) is sandwiched between two 125 μ m matte-polyester substrates. These polyester layers prevent the formation of Newton ring interference patterns, when the irradiated EBT3 films are scanned with flatbed scanners [16]. We use an EPSON Expression 11000XL scanner, with a resolution of 4800 dpi in transmission mode. The scanned area of each film is about 0.5×0.5 cm². The scanned images are then converted into 8 bits grey scale and processed with ImageJ software, in order to convert the pixel values into standard optical density values. High precision calculation of the optical density for each irradiated film is essential to determine the exact values of the radiation doses inside the interaction chamber.

The EBT3 films are previously calibrated using 40 kV X-rays [17]. The dosimetry measurements are performed using a plane parallel chamber connected to a UNIDOS Secondary Standard Dosimeter, previously calibrated to a PTB primary standard. The resulting calibration graph is shown in Fig. 2.

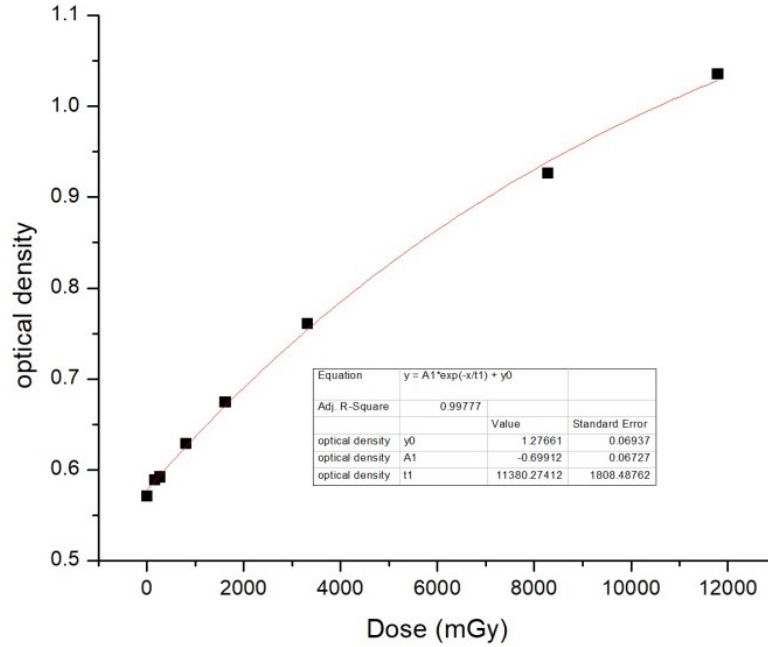


Fig. 2: Optical density dependence on radiation dose. Black points correspond to measurements performed, the fitting curve is red. Fit parameters are supplied in the figure legend.

3.3. Experimental map of the measured doses inside the target chamber

The interaction of high-power lasers with thin solid targets generates proton, electron, X-ray radiation and neutron fluxes that span a wide energy range [6, 18, 19]. Laser accelerated electrons that interact with the walls of the target chamber produce X-ray bremsstrahlung radiation [6]. In the experiments described in the previous section, we chart the radiation dose distribution inside the interaction chamber. Fig. 3 shows the map of the radiation dose measured inside the interaction chamber for a laser intensity of 5×10^{19} W/cm². The dose values recorded are per shot and are normalized with respect to a 30 cm distance (with respect to the laser-target interaction point). The maximum radiation dose is reached in a direction normal to the target surface.

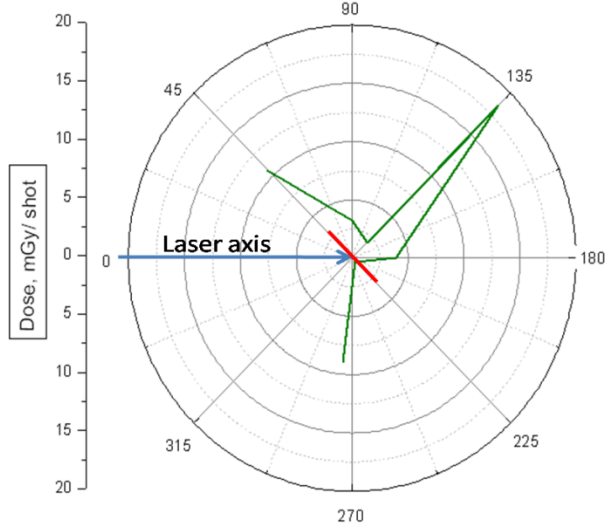


Fig. 3: Map of measured doses per shot, at 30 cm apart from the laser-target interaction point, recorded inside the interaction chamber, for a laser intensity value of $5 \times 10^{19} \text{ W/cm}^2$.

The radiation doses inside the interaction chamber measured per laser shot (during the experiments previously presented), are similar to those measured outside spacecrafts and space stations [13, 20-23]. Good knowledge of the radiation field background and doses outside spacecraft is important in order to estimate the inner radiation field. In Ref. [22], average values of hundreds of μGy were measured and reported for daily cumulative radiation doses inside spacecraft cabins.

Testing of electronic systems and software intended to be used in space is preferably performed on Earth in dedicated facilities, in order to overcome problems that are inherent in space dosimetry. The mixed radiation environment generated in high power laser - thin solid target experiments can simulate the aggressive space environment specific to space stations and spacecraft cabin habitats, as it is extremely important to test and optimize different shielding materials and structures [24].

3.4. Simulation model of the experimental radiation map

The experimental conditions enable one to reconstruct the radiation field within the interaction chamber, which allows us to characterize specific radiation conditions (such as particle flow and dose) for any point in space. Dose reconstruction has been achieved by radiation transport simulations using the Geant4 V.10.5 framework. In order to obtain a realistic simulation, two volume sources are considered.

The first source would be the pre-plasma obtained due to the interaction of the PW laser with the target surface. Hot, relativistic electrons are generated with a temperature of 2.8 MeV. The source is considered to exhibit a uniform angular distribution and a Gaussian

energy distribution. The source location is chosen in front of the target, on the opposite side with the pre-plasma [8, 25, 26]. In Fig. 4a, the pre-plasma is illustrated as a yellow disk while the red disk represents the target. The energy of the laser accelerated electrons is estimated to be around 17 MeV.

The second source considered in simulations is the proton source that has a narrow angular distribution along the normal drawn to the target back surface. The proton spectral distribution is estimated considering the Target Normal Sheath Acceleration (TNSA) model [8, 18, 19]. The maximum proton energy depends on the target thickness, and it is approximately 16.7 MeV for a 10 μm Al target [20, 27].

These two sources are simultaneously implemented using the Geant4 General Particle Source module, with a 10:1 ratio of the relativistic electron source with respect to the proton source. Besides the proton and electron sources, the mesh of the simulation geometry (see Figure 4a) includes the exact parameters of the experimental setup shown in Fig. 1. The protons that originate from the source propagate through the environment, and undergo nuclear reactions when they interact with the experimental setup within the simulation region, generating secondary radiation such as photons and electrons. The electron and photon fluencies that result are presented in Fig. 4b and 4c.

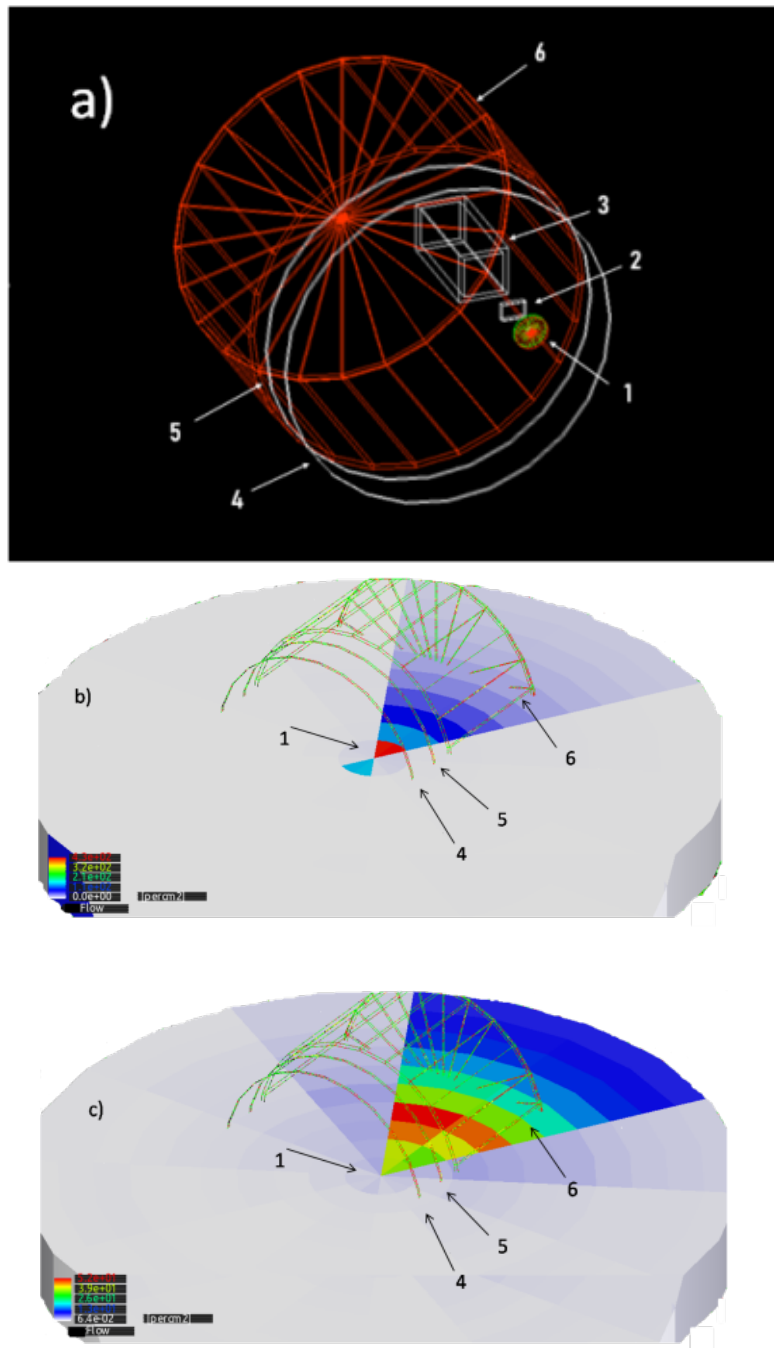


Figure 4: a) Geometry Mesh of the GEANT4 simulation: 1 - sources of laser accelerated electrons and protons; 2 - hole; 3 - magnetic spectrometer; 4 - target holder; 5 - detector holder; 6 - aluminum cylinder b) Simulated electron fluencies; c) Simulated photon fluencies.

4. Method to increase the proton energy spectrum resolution

A patent application was submitted [Patent Application, OSIM A/00337/05.06.19], that refers to a method used to determine the energy distribution of a proton beam. The method, while not being limited to, can be applied to diagnose protons that are (i) generated owing to

the interaction between a plasma and a high power laser beam, (ii) present in cosmic radiation, or (iii) medical equipment employed for proton therapy, etc.

One of the methods used to detect protons consists in using solid media, specifically designed for this purpose and produced as foils that are exposed to a flux of protons. Currently, the most prevalent substance used to this end is *poly allyl diglycol carbonate* ($C_{12}H_{18}O_7$) commercially known as CR-39. The protons crossing these detectors deteriorate the structure of the material, and leave physical traces in the form of sensitized areas of energetic electrons that emerge as an outcome of the interaction between the proton and the foil material. They represent electrons that are “extracted” from the atoms, with a specific energy that dissipates in the neighbouring regions. These electrons sensitize the physical structure of the material by breaking some of the chemical bonds thus rendering the material easier to corrode in the specific etching process. Different etching agents are used, such as NaOH or KOH. The etching agent acts upon the foil (detector) surface, as the corrosion rate is higher for sensitized areas where blowholes appear that are visualized and counted using a microscope. In Ref. [20] a method is described to determine the energetic spectrum of protons at normal incidence on a CR-39 detector, based on counting the blowholes generated by the protons. For a 1 mm thick CR-39 plate, an upper limit of the maximum energy is reported at 7.5 MeV. The analysis of the blowholes on the back of the plate indicates the presence of protons with energies of about 10 MeV.

Owing to a variation of the proton stopping position by tenths of microns, caused by statistical fluctuations of the proton energy transfer towards the material they cross, blowholes with different dimensions occur for a 20 micron etching, even if they result from protons of equal energy. This represents a proof that protons can exhibit energies larger than 10 MeV. Protons that cross into the second CR-39 detector leave identifiable traces only on the back surface of the first detector. Nevertheless, these protons can be identified by analysing the traces left on the front surface of the second CR-39 detector, according to the method suggested in [13]. The paper also shows the problems associated with determining the energetic spectrum for protons with energies between $7.5 \div 10$ MeV. In order to obtain reproducible results, the etching conditions such as time of application, concentration, and temperature, should be identical. By analysing the shape and dimensions of the traces, one can determine the energy and the direction of motion for incident protons. According to Ref. [21], by using 1500 μm thick CR-39 nuclear track detectors, it is possible to determine the proton energy distribution in the domain $0.92 \div 9.28$ MeV. Moreover, late experiments [28] show that a preliminary calibration procedure of the detector stack is mandatory.

Accurate determination of the proton energetic spectrum, and particularly of the maximum energy acquired after the laser-pulse solid target interaction, enables one to estimate the electron temperature as shown in [8]. This issue is very important for developing

applications of interest for Radiation Hardness Assurance (RHA), by simulating the aggressive radiation environment from the outer space by means of laser plasma accelerators [6]. The method supplies information about the characteristics of individual protons. Nevertheless, the method described in [6, 8] also presents some disadvantages such as:

- determination of incident proton characteristics is done only for particles whose energy lies within a specified value range
- in order to visualize and measure the trace dimensions at the foil, the etching process must be performed in several steps, at well defined intervals of time. After each step the foil surface is optically examined then the etching process is resumed, which finally leads to an increase of the processing time

The method proposed to determine the energetic spectrum of protons is based on using a set of solid detectors, preferably CR-39 [13]. Each detector is thinner than the Bragg peak that characterizes the loss of kinetic energy as a function of the particle track in the detector material. The Bragg peak is characterized by an intense peak whose position is a clear indication of the particle location where the particle loses the largest part of its kinetic energy. For protons the Bragg peak occurs right before stopping. The method we devised circumvents some of the disadvantages associated with previous methods, and brings in the following advantages [13]:

- it enhances the resolution used to determine the proton energy and extends the interval of energy values for which the method is applicable. This characteristics is useful for proton beams with energy spread over a wide range of values
- the etching process is simultaneously performed for all solid detectors. Consequently, etching is performed faster, under identical conditions for all solid CR-39 detectors. Each detector is etched once.

The thickness of the Bragg peak region is defined as the full width at half maximum (FWHM) of the energy loss curve, that describes the specific energy deposition dE/dx of a heavy charged particle as a function of the penetration depth. For proton energies in the 3 ÷ 14.8 MeV range it is about 0.2 mm. Thus, the thickness of the CR-39 detector should not exceed 0.2 mm.

As an example of applying this method to determine the proton energy spectrum, a stack of 10 CR-39 200 μm thick detectors is used. The stack is wrapped within a 10 μm thick aluminium foil for protection. A preliminary calibration procedure is mandatory, using protons with well known energy. This could be for instance achieved by using the accelerators located at IFIN-HH (<http://www.nipne.ro/>), that are able to generate protons of 2, 3 and 5 MeV. Moreover, an accelerator can be used that delivers protons with an energy of 12 MeV. By using a monoenergetic proton source one can obtain an exponential proton energy spectrum. The detector system (presented in [13]) consists of a rotating disk holding

the targets, placed in front of the detector stack. Filters that consist of metallic foils are interposed between the front of the detector stack and the proton source. The maximum energy of the protons incident on the detector stack is obtained when it is directly exposed to the action of the protons generated by the proton source, in absence of any filter. Lower energies result when the protons pass through different filters, that are consecutively interposed between the proton source and the detector pack, using a mechanical system, preferably a rotating one. Passive detectors such as CR-39 are time independent, thus if the proton flux is low enough for avoiding nonlinear effects they behave as if all protons arrived at the same time. In such conditions, calibration is performed by exposing the CR-39 stack to a flux of protons at normal incidence, and the fluence is tuned such that the blowholes do not overlap. The detectors are etched using a classical procedure [13], then optical microscopy is used to analyse the traces left on both front and back faces of the solid detector. The number of blowholes on each face of the detector is counted and analysed, in order to emphasize experimental patterns. Results are verified by comparison with those reported in [20]. The protons lose 1 MeV when crossing the Al foil. Measurement errors are determined by considering previously performed calibrations.

5. Conclusions

We report on measurements of the radiation dose distribution map inside a target chamber during laser proton acceleration experiments using thin solid targets. We estimate the maximum energy of the protons as approximately 14 MeV.

An integrated dose of about 15 mGy was observed per laser shot along the direction normal to the target, at 30 cm distance from the laser-target interaction point. This dose is due to a mixed photon and electron radiation field. A mesh of the experimental set-up geometry is generated and used as input for computing the radiation doses around the interaction point, by using the Geant4 General Particle Source code. The resulting radiation doses map shows good agreement with the experimental values.

The experimental and simulation results obtained suggest that high power laser - thin solid target experiments can be used as a test environment for electronics and software equipment supposed to be deployed in spacecraft and space station habitats.

For the particular geometry described here we find a reasonable agreement between measurements and simulations, which validates the numerical simulations implemented by our code. We extend our assumption and claim that the code can also be used for other type of radiation sources to simulate radiation inside and near space stations, at least by considering a superposition of radiation fields, if nonlinear effects can be neglected. Even if the space radiation background is pseudo-continuous, while the one generated in laser - target interaction experiments comes in short pulses, the key advantage of laser - plasma

interaction is that it can generate simultaneously protons, X-rays and electrons. The good agreement between the experimental and simulation data reported here, leads to the possibility of applying the simulation tools to characterize and simulate new shielding materials and designs of present interest.

To increase the resolution of the proton energy spectrum determination, a new method is developed, characterized by using plastic foil stacks (preferably CR-39), but not limited to. The thickness of each foil should be less than the one of the major specific energy deposition region of a proton, i.e. around the Bragg peak. This method for determining the proton energy spectrum is characterized by using stacks of plastic foils for which the etching is performed on each face, to a depth of less than 20 μm , avoiding damage of the foil's mechanical characteristics.

The number of protons stopped in each foil is assessed by analysing the number of pits corresponding to the protons stopped on the front side of the foil. Only those tracks are considered that have a diameter larger than a certain value, which is characteristic for tracks induced by protons at the limit of stopping, when passing through a given foil. Particularly, the plastic film stack could be used to determine the proton energy spectrum when testing the effect of proton fluxes on electronic components. This plastic foil stack could also be used for the characterization of laser accelerated protons and for medical applications (e.g., proton therapy), as well as for monitoring certain environments which are subject to ionizing radiation, such as space stations, ships and shuttles, especially during solar storms or the passage of a space vehicle through the radiation belts of some planets in the solar system. The stacks of plastic films can be calibrated with proton beams of known energy distribution, generated in classical or modern proton accelerators. A mechanical device could be used to rapidly interpose various filters between the calibration proton source and the foil stack. This way, the energy of protons reaching the stack is reduced, in a known and controllable way. The proton energy spectrum is determined based on the analysis of protons stopped in each foil. Due to the low foil thickness a well defined energy can be assigned to each of them, based on its position within the stack. The total number of protons incident on the stack front surface is obtained by summing up the number of protons stopped in each of the foils. The resolution of the assessed proton energy spectrum can be achieved by analysing the track diameters on the foils.

Conflicts of Interest: The authors declare no conflict of interest. The funders had no role in the design of the study; in the collection, analyses, or interpretation of data; in the writing of the manuscript, or in the decision to publish the results.

Acknowledgments: We acknowledge support from the CETAL-PW facility at the National Institute for Laser, Plasma and Radiation Physics, Magurele, Romania and fruitful discussions with Dr. Șerban Udrea from GSI-Darmstadt.

Funding: This work has been funded by European Space Agency within the ESA contract No.4000121912/17/NL/CBi by Romanian National Authority for Scientific Research and Innovation, contract No. 3N/2018 (Project PN 18 13 01 03) and by Romanian Space Agency, contract No. 53/19. 11. 2013 (Competence Center: Laser-Plasma Acceleration of Particles for Radiation Hardness Testing - LEOPARD)

References

- [1] Holly Zell, National Aeronautics and Space Administration, Page Last Updated: Aug. 4, 2017, https://www.nasa.gov/mission_pages/rbsp/science/rbsp-spaceweather.html
- [2] D. N. Baker, S. G. Kanekal, V. C. Hoxie, M. G. Henderson, X. Li, H. E. Spence, S. R. Elkington, R. H. Friedel, J. Goldstein, M. K. Hudson, G. D. Reeves, R. M. Thorne, C. A. Kletzing, and S. G. Claudepierre. *A long-lived relativistic electron storage ring embedded in Earth's outer Van Allen belt*, Science **340** (6129):186–190, April 2013.
- [3] Cannon, P. (2013). *Extreme space weather: impacts on engineered systems and infrastructures*. In Royal Academy of Engineering. Retrieved from [http://www.raeng.org.uk/news/publications/list/reports/Space Weather Full Report Final.PDF](http://www.raeng.org.uk/news/publications/list/reports/Space_Weather_Full_Report_Final.PDF)
- [4] Delzanno, G. L., Borovsky, J. E., Thomsen, M. F., Moulton, J. D., & Macdonald, E. A. (2015). *Future beam experiments in the magnetosphere with plasma contactors: How do we get the charge off the spacecraft?* Journal of Geophysical Research: Space Physics, 120(5), 3647–3664. <https://doi.org/10.1002/2014JA020608>
- [5] Ticoș, D., Scurtu, A., Oane, M., Diplășu, C., Giubega, G., Călina, I., & Ticoș, C. M. (2019). *Complementary dosimetry for a 6 MeV electron beam*. Results in Physics, 14(February), 102377. <https://doi.org/10.1016/j.rinp.2019.102377>
- [6] T. Koenigstein et al., *Design considerations for the use of laser-plasma accelerators for advanced space radiation studies*, Journal of Plasma Physics 78 (4), 383 - 391 (2012) <https://doi.org/10.1017/S0022377812000153>
- [7] Macchi, A., Borghesi, M., & Passoni, M. (2013). Ion acceleration by superintense laser-plasma interaction. Reviews of Modern Physics, 85(2), 751–793. <https://doi.org/10.1103/RevModPhys.85.751> (2013)

- [8] Tampo, M., Awano, S., Bolton, P. R., Kondo, K., Mima, K., Mori, Y., ... Kodama, R. (2010). Correlation between laser accelerated MeV proton and electron beams using simple fluid model for target normal sheath acceleration. *Physics of Plasmas*, 17(7). <https://doi.org/10.1063/1.3459063> (2010)
- [9] Danson, C., Hillier, D., Hopps, N., & Neely, D. (2015). Petawatt class lasers worldwide. *High Power Laser Science and Engineering*, 3(January). <https://doi.org/10.1017/hpl.2014.52>
- [10] Center for Advanced Laser Technologies (CETAL), Ultra-intense Lasers Laboratory; <http://cetal.inflpr.ro/newsite/cetal-pw>
- [11] T. Asavei, M. Tomut, M. Bobeica, S. Aogaki, M. O. Cernaianu, M. Ganciu, S. Kar, G. Manda, N. Mocanu, L. Neagu, C. Postolache, D. Savu, D. Stutman, D. Vizman, D. Ursescu, S. Gales, N. V. Zamfir, *Materials in extreme environments for energy, accelerators and space applications at ELI-NP*, Romanian Reports in Physics, **68**, Supplement, P. S275–S347 (2016)
- [12] Ganciu, M.; Groza, A.; Cramariuc, O.; Mihalcea, B.; Serbanescu, M.; Stancu, E.; Surmeian, A.; Butoi, B.; Dreghici, D.; Chiroasca, A.; Cramariuc, B.; *Hardware and software methods for radiation resistance rising of the critical infrastructures*. Rom. Cyber Secur. J. **1**, 3–13 (2019)
- [13] A. Groza, M. Serbanescu, B. Butoi, E. Stancu, M. Straticiuc; I. Burducea, A. Balan, A. Chiroasca, B. Mihalcea, M. Ganciu, *Advances in Spectral Distribution Assessment of Laser Accelerated Protons using Multilayer CR-39 Detectors*, Appl. Sci. **9**, 2052 (2019); <https://doi.org/10.3390/app9102052>
- [14] G. Giubega, Proton acceleration in ultra-intense laser interaction with solid targets at CETAL-PW laser, Poster presentation, **Workshop CETAL 2018**, <http://cetal.inflpr.ro/newsite/workshop>
- [15] J. Allison *et al*, *Recent developments in Geant4*, Nucl. Instrum. Meth. Phys. Res. A: Accelerators, Spectrometers, Detectors and Associated Equipment **835**, p. 186 - 225, <https://doi.org/10.1016/j.nima.2016.06.125> (2016) .
- [16] Monsen Najafi, Ghazale Geraily, Alireza Shirazi, Mahbod Esfahani, Javad Teimouri, Analysis of Gafchromic EBT3 film calibration irradiated with gamma rays from different systems: Gamma Knife and Cobalt-60 unit, Medical Dosimetry 2017
- [17] <http://tomography.inflpr.ro/>
- [18] Hidding, B., Karger, O., Königstein, T., Pretzler, G., Manahan, G. G., McKenna, P., R. Gray, R. Wilson, S. M. Wiggins, G. H. Welsh, A. Beaton, P. Delinikolas, D. A. Jaroszynski, J. B. Rosenzweig, A. Karmakar, V. Ferlet-Cavrois, A. Costantino, M. Muschitiello, Daly, E. (2017) *Laser-plasma-based Space Radiation Reproduction in the Laboratory*. Scientific Reports, 7 (February), 1–6. <https://doi.org/10.1038/srep42354>

- [19] J. Fuchs, P. Antici, E. d'Humieres, E. Lefebvre, M. Borghesi, E. Brambrink, C. A. Cecchetti, M. Kaluza, V. Malka, M. Manclossi, S. Meyroneinc, P. Mora, J. Schreiber, T. Toncian, H. Pepin, and P. Audebert (2006). Laser-driven proton scaling laws and new paths towards energy increase. *Nature Physics*, 2(1), 48–54. <https://doi.org/10.1038/nphys199>
- [20] T. W. Jeong *et al.*, *CR-39 track detector for multi-MeV ion spectroscopy*, **Scientific Reports**, 7:2152 (2017)
- [21] N. Sinanian *et al.*, *The response of CR-39 nuclear track detector to 1-9 MeV protons*, **Rev. Sci. Instrum.**, 82, 103303 (2011)
- [22] Zhou, D., Sullivan, O. D., Semones, E., Zapp, N., Wang, S., Liu, S., Zhang B., Ye Z., Reitz G., Berger T., Benton, E. R. (2011). *Radiation of Cosmic Rays Measured on the International Space Station 1 Introduction 2 LET Spectr um Method 3 Matroshka Experiments*. 6, 107–110. <https://doi.org/10.7529/ICRC2011/V06/1248>
- [23] M. Ganciu, M.-I. Piso, O. Stoican, B. Mihalcea, C. Diplasu, O. Marghitu, A. Julea, A. Surmeian, A. Groza, R. Dabu, I. Morjan, Application System and method for testing components, circuits and complex systems using synchronized and pulsed fluxes consisting of laser accelerated particles, Patent Application, WO201503061 A1, WO2015030619A4 (2015)
- [24] Narici, L., Casolino, M., Fino, L. Di, Larosa, M., Picozza, P., Rizzo, A., & Zaconté, V. (2017). *Performances of Kevlar and Polyethylene as radiation shielding on-board the International Space Station in high latitude radiation environment*. *Scientific Reports*, (March), 1–11. <https://doi.org/10.1038/s41598-017-01707-2>
- [25] Xiao, K. D., Zhou, C. T., Jiang, K., Yang, Y. C., Li, R., Zhang, H., ... He, X. T. (2018). *Multidimensional effects on proton acceleration using high-power intense laser pulses*. *Physics of Plasmas*, 25(2). <https://doi.org/10.1063/1.5003619>
- [26] Volpe, L., Fedosejevs, R., Gatti, G., Pérez-Hernández, J. A., Méndez, C., Apiñaniz, J., ... Roso, L. (2019). *Generation of high energy laser-driven electron and proton sources with the 200 TW system VEGA 2 at the Centro de Laseres Pulsados*. *High Power Laser Science and Engineering*, 7, 6–11. <https://doi.org/10.1017/hpl.2019.10>
- [27] Fuchs, J., Antici, P., D'Humières, E., Lefebvre, E., Borghesi, M., Brambrink, E., ... Audebert, P. (2006). *Laser-driven proton scaling laws and new paths towards energy increase*. *Nature Physics*, 2(1), 48–54. <https://doi.org/10.1038/nphys199>
- [28] Y. Zhang *et. al*, *Energy calibration of a CR-39 nuclear-track detector irradiated by charged particles*, **Nucl. Sci. Tech.**, 30: 87 (2019)